Astron. Astrophys. 328, 343–348 (1997)

ASTRONOMY AND ASTROPHYSICS

An operator perturbation method for polarized line transfer

II. Resonance polarization with partial frequency redistribution effects

Frédéric Paletou and Marianne Faurobert-Scholl

Observatoire de la Côte d'Azur, Département Cassini (CNRS/UMR 6529), B.P. 4229, F-06304 Nice Cedex 4, France

Received 7 July 1997 / Accepted 22 July 1997

Abstract. The effects of partial frequency redistribution are implemented in the Polarized Accelerated Lambda Iteration (PALI) method of Faurobert-Scholl et al. (1997). The numerical scheme is an extension of the core-wing technique of Paletou & Auer (1995) originally developed for non-polarized line transfer problems. Using a new code, we validate theoretical results against those given by a Feautrier type code.

Key words: line: formation – polarization – radiative transfer – methods: numerical – stars: stmospheres

1. Introduction

During the last decade, efficient iterative methods have been developed for the solution of non-LTE radiative transfer problems. They are generally referred to as Accelerated Lambda Iteration (ALI) methods. They are basically operator splitting methods. In order to derive the iterative scheme, one introduces an approximate of the full Λ operator - which gives the radiation field from a known source function.

In a seminal paper, Olson et al. (1986, hereafter OAB) pushed the ALI method to the limit of using a local approximate operator. The latter is simply the diagonal of the full Λ operator. Initially developed for the schematic non-LTE two-level atom (unpolarized) radiation transfer problem with complete frequency redistribution (CRD), the OAB method was quickly extended to partial frequency redistribution (PRD) problems (Auer & Paletou 1994, Paletou & Auer 1995), multi-dimensional problems (Auer & Paletou 1994, Auer et al. 1994, Väth 1994) and multilevel atom problems (Rybicki & Hummer 1991, Auer et al. 1994, Paletou 1995).

More recently, the OAB method has been generalized to polarized radiation transfer in a non-magnetic regime (Faurobert-Scholl et al. 1997; hereafter Paper I) and also to the case of weak magnetic field regime (Nagendra et al. 1997) in 1D media for the case of CRD. However, for many strong resonance lines of astrophysical interest, the effects of PRD definitely have to be taken into account (see e.g. Faurobert-Scholl 1992, 1994).

In this article we show that the ALI-based method for PRD problems developed by Paletou & Auer (1995) can be successfully implemented in the PALI scheme of Faurobert-Scholl et al. (1997). Hereafter we consider only the case of polarization in the non-magnetic field regime i.e *resonance polarization*.

In Sect. 2 we summarize the derivation of the PRD method of Paletou & Auer (1995). For simplicity, the method is written for the scalar i.e. unpolarized radiation transfer problem. Then we describe in Sect. 3 the implementation of that iterative scheme in the framework of the PALI formalism. Finally in the following sections, two theoretical test cases are presented. We discuss the convergence properties and compare our results with those given by a Feautrier type code (Faurobert 1987).

2. The CRDCS scheme

The two-level atom line source function S_x may be defined as

$$S_x = (1-\varepsilon)\bar{J}_x + S^*_x \ , \tag{1}$$

where ε is the collisional destruction probability, S^* the primary source of photons and $\bar{J}_x$ the PRD scattering integral given by

$$\bar{J}_x = \frac{1}{2}\int_{-1}^{+1} d\mu \int_{-\infty}^{+\infty} \left[\frac{R_{xx'}}{\phi_x}\right] I_{x'\mu} dx' \ . \tag{2}$$

Note that the complete frequency redistribution case is recovered when one assumes decorrelation between the absorption (x') and emission frequencies (x), i.e. $R_{xx'} = \phi_x \phi_{x'}$. In this case, the scattering integral $\bar{J}_x$ is frequency independent, unlike in PRD.

Hereafter, we consider only the case of coherent scattering in the atom's frame described by the frequency redistribution function R_{II-A} (Hummer 1962). We also restrict the present study to the case of *angle-averaged* frequency redistribution in a *static* media. The properties of R_{II-A} can be found in classic textbooks (e.g. Jefferies 1968, Mihalas 1978).

The CRDCS scheme for PRD assumes a CRD approximation over the Doppler core and Coherent Scattering in the line

Send offprint requests to: paletou@obs-nice.fr

wings. It was introduced by Paletou & Auer (1995; hereafter PA95) for non-polarized radiation transfer problems. Let us now recall the elements of that method.

In PRD, the formal solution of the radiative transfer equation can be written as

$$\bar{J}_x = \mathscr{S}_x[S_x] \ . \tag{3}$$

The major argument of the CRDCS scheme relies on the fact that, for $\mathrm{R_{II-A}}$ redistribution it is physically justifiable to introduce the following approximate operator

$$\mathscr{S}^*_x[\ ] = (1-\alpha_x)\int_{\rm core} \phi_{x'}\Lambda_{x'}[\ ]dx' + \alpha_x\int_{\rm wing}\delta(x-x')\Lambda_{x'}[\ ]dx' \ , \tag{4}$$

where, according to the standard formalism used in the field of radiation transfer, Λ_x is the *monochromatic* operator giving the angle-averaged mean intensity from a known source function:

$$J_x = \Lambda_x[S_x] \ . \tag{5}$$

This choice is recommended in PA95. The splitting coefficients $\{\alpha_x\}$ are simply the diagonal elements of the redistribution matrix $\hat{g}$ over the "wing domain" and zero elsewhere. This particular choice was made in order to switch smoothly from CRD in the Doppler core to coherent scattering in the far wings (see PA95; Fig. 5); $\hat{g}$ is the frequency weights matrix appearing in the PRD scattering integral expression in a discrete form:

$$\int_{-\infty}^{+\infty}\left[\frac{R_{xx'}}{\phi_x}\right]J_{x'}dx' = \sum_{j=1}^{N_{\rm freq}} g_{ij}J_j \ . \tag{6}$$

Thus, we can derive an iterative scheme assuming the perturbations:

$$\begin{cases} S_x^{(n+1)} = S_x^{(n)} + \delta S_x^{(n)} \\ \mathscr{S}_x[\ ] = \mathscr{S}^*_x[\ ] + (\mathscr{S}_x - \mathscr{S}^*_x)[\ ] \ . \end{cases} \tag{7}$$

The equation for the line source function corrections follows in a straightforward fashion:

$$\delta S_x^{(n)} - (1-\varepsilon)\mathscr{S}^*_x[\delta S_x^{(n)}] = r_x^{(n)} \ , \tag{8}$$

where the residuals $r_x^{(n)}$ are defined as

$$r_x^{(n)} = (1-\varepsilon)\mathscr{S}_x[S_x^{(n)}] + S_x^* - S_x^{(n)} \ . \tag{9}$$

At this point we need to consider separately two different frequency domains according to the properties of the $\mathrm{R_{II-A}}$ frequency redistribution function.

2.1. The core domain

In the Doppler core i.e. around line center, departures from CRD are small and the approximation $R_{xx'} \simeq \phi_x\phi_{x'}$ is satisfactory. As proposed in PA95, at core frequencies ($x \le x_c$) the splitting coefficients α_x are set to zero.

Therefore, in this frequency domain the line source function increments should satisfy the equation

$$\delta S_x^{(n)} - (1-\varepsilon)\int_{\rm core}\phi_x\Lambda_x[\delta S_x^{(n)}]dx = r_x^{(n)} \ , \tag{10}$$

which can be solved following a method similar to the ones adopted by Scharmer (1983) and Auer & Paletou (1994).

At core frequencies, the line source function increments are thus given by the sum of a frequency dependent residual $r_x^{(n)}$ plus a frequency independent term ΔT defined as:

$$\Delta T = (1-\varepsilon)\int_{\rm core}\phi_x\Lambda_x[\delta S_x^{(n)}]dx \ . \tag{11}$$

Integrating Eq. (10) over the core, we can write a new equation enabling us to evaluate ΔT. Then introducing the diagonal operator Λ^*_x and using the first order approximation $\Lambda_x[\delta S] \simeq \Lambda^*_x[\delta S]$, the frequency independent correction ΔT may be calculated at each point in the grid by

$$\Delta T = [1-(1-\varepsilon)\bar{\Lambda}^*]^{-1}\left[(1-\varepsilon)\int_{\rm core}\phi_x\Lambda_x[r_x^{(n)}]dx\right] \ , \tag{12}$$

where $\bar{\Lambda}^*$ is the approximate local operator weighted by the absorption profile and integrated over the core domain.[1] And finally the line source function increments are evaluated according to the following expression:

$$\delta S_x^{(n)} = \Delta T + r_x^{(n)} \ . \tag{13}$$

2.2. The wing domain

For $\mathrm{R_{II-A}}$ frequency redistribution, scattering becomes quasi-coherent in the line wings. The splitting coefficients $\{\alpha_x\}$ ensure a smooth transition from CRD (in the Doppler core) to the quasi-coherent photon's scattering regime in the far wings.

The great advantage of the CRDCS scheme is that the source function increments are very easily evaluated in the wing domain. Indeed, at each frequency the source function correction is merely

$$\delta S_x^{(n)} = [1-\alpha_x(1-\varepsilon)\Lambda^*_x]^{-1}[r_x^{(n)} + (1-\alpha_x)\Delta T] \ , \tag{14}$$

once ΔT has been previously evaluated.

3. Implementation of CRDCS in PALI

The PALI method was developed in the matrix formalism introduced by Ivanov and his co-workers (Ivanov 1995, Ivanov et al. 1995). We refer the reader to Paper I for details which we shall not fully recall below.

Theoretical test cases we present hereafter concern *resonance polarization* i.e. line polarization in a non-magnetic

[1] When the integration in frequency is performed over the full absorption profile, the operator $\bar{\Lambda}^*$ is identical to the local operator introduced by Olson, Auer & Buchler (1986).

regime. We also consider axially symmetric polarized radiation fields which may be described by a *two-component* vector $\boldsymbol{I} = (I, Q)^{\mathrm{T}}$ where I and Q are the two Stokes parameters describing intensity and linear polarization, respectively. The source function is also a vector $\boldsymbol{S}$ which, in the case of resonance polarization can be factorized as

$$\boldsymbol{S}(x,\tau,\mu) = \hat{A}(\mu)\boldsymbol{P}(x,\tau) \ , \tag{15}$$

where $\hat{A}$ is a (2×2) matrix and $\boldsymbol{P}$ a two-component column vector depending *only* on frequency and optical depth (Rees 1978).

As in Paper I, we shall use a formalism for which the source function $\hat{S}$ is a (2×2) matrix; it is related to the vector quantity by

$$\boldsymbol{S}(x,\tau,\mu) = \hat{A}(\mu)\hat{S}(x,\tau)\boldsymbol{e} \ , \tag{16}$$

where $\boldsymbol{e} = (1,1)^{\mathrm{T}}$. It follows from the previous equations the relation between $\boldsymbol{P}$ and $\hat{S}$,

$$\boldsymbol{P}(x,\tau) = \hat{S}(x,\tau)\boldsymbol{e} \ . \tag{17}$$

3.1. The matrix scattering integral

$\hat{S}$ is related to the mean intensity by an expression which is formally identical to Eq. (1) although the angular averaging of the specific intensity matrix $\hat{I}$ now involves $\hat{A}$ and its transpose $\hat{A}^{\mathrm{T}}$ (see also Eq. (21) in Paper I). Indeed, the scattering integral is also a (2×2) matrix which can be defined as

$$\widehat{\bar{J}}_x = \frac{1}{2}\int_{-1}^{+1} \hat{A}^{\mathrm{T}}(\mu)\hat{A}(\mu)d\mu \int_{-\infty}^{+\infty} \left[\frac{R_{xx'}}{\phi_x}\right] \hat{I}_{x'\mu}dx' \ . \tag{18}$$

Following Ivanov (1995) and Faurobert-Scholl et al. (1997), we introduce the $\hat{A}$ matrix given by

$$\hat{A}(\mu) = \begin{pmatrix} 1 & \sqrt{\frac{W_2}{8}}(1-3\mu^2) \\ 0 & \sqrt{\frac{W_2}{8}}3(1-\mu^2) \end{pmatrix} \ . \tag{19}$$

Therefore, existing ALI-based codes can be easily extended to PALI codes by modifying the formal solution solver for handling (2×2) matrices instead of a scalar source function. In our study, we used the short characteristics method (Auer & Paletou 1994) in the formal solution solver.

3.2. The primary source term in PRD

The primary source term in its matrix form, $\hat{S}^*$, can be evaluated according to Faurobert-Scholl et al. (1997) although in the general case of PRD, each component of the $\hat{S}^*$ matrix is now frequency dependent. Non-diagonal elements are zero and the diagonal ones are defined as

$$\begin{aligned} S^*_{11}(x,\tau,\mu_0) \ = \ & \frac{(1-\varepsilon)}{2} I^{inc}[M(x,\tau,\mu_0) \\ & + M(x,T-\tau,\mu_0)] \end{aligned} \tag{20}$$

and

$$\begin{aligned} S^*_{22}(x,\tau,\mu_0) \ = \ & \sqrt{\frac{W_2}{8}}[(1-3\mu_0^2) \\ & + 3p^{inc}(1-\mu_0^2)]S^*_{11}(x,\tau,\mu_0) \ , \end{aligned} \tag{21}$$

where μ_0 is the direction cosine of the incident beam on both sides of the finite slab, T the total optical depth and I^{inc} and p^{inc} are respectively the intensity and polarization of the incident radiation field. It is important to note that, in PRD, the expression given in Eq. (27) of Paper I becomes

$$M(x,\tau,\mu_0) = \int_{-\infty}^{+\infty} e^{-\tau\phi(x')/|\mu_0|} \left[\frac{R_{xx'}}{\phi_x}\right] dx' \ . \tag{22}$$

3.3. Optical depth grids

Using a fine mesh for the optical depth (more than 7 points/decade) we find strong *local* instabilities due to sign changes in the polarized components of $\hat{S}$. This effect is always likely to arise in PRD because, in general, one may expect at least one zero to occur for at least one of the polarized components of $\hat{S}$ at each frequency!

A two-level grid-doubling strategy provides a practical solution, although crude, to this particular problem. At the change of grid level, we initially double the coarse (level 1) grid. However, before interpolating the coarse grid solution for $\hat{S}$ onto the new grid, we seek the zeros of the matrix source function elements. Then we *remove* new grid points close to those zeros which exist in intervals (of the coarse grid) such that the source function value at one end of the interval is smaller in absolute value than ϵ_{c}. We adopt for ϵ_{c} the smallest single precision floating point value available on most computers (5.96×10^{-8}).

With this "trick" we therefore do not double the coarse grid in a uniform manner. Results shown below were obtained starting with a 4.5 points/decade grid resolution. In both cases, after filtering out the actual zeros of the polarized source function components, the second grid get an average resolution close to 8 points/decade. We insist on the fact that we could not get a *direct* solution with the latter optical depth resolution. The implementation of a grid adaptation algorithm - numerical techniques which are well known in the field of hydrodynamics for instance (see e.g. Dorfi & Drury 1987) - should provide a more elegant and efficient way of handling what seems to be an intrinsic flaw of the PALI method.

4. Theoretical test cases

We assume two different test cases adapted from those introduced in Sect. 4.2 of Paper I to the PRD problem. CASE I considers a self-emitting and isothermal finite slab while CASE II describes a finite slab illuminated on both sides by an external radiation field.

The slabs are monodimensional and characterized by their total optical thickness $T = 2 \times 10^9$. The frequency grid in PRD has 65 points over a half-profile from line center up to 10^3 Doppler widths away; it is equally spaced across the Doppler

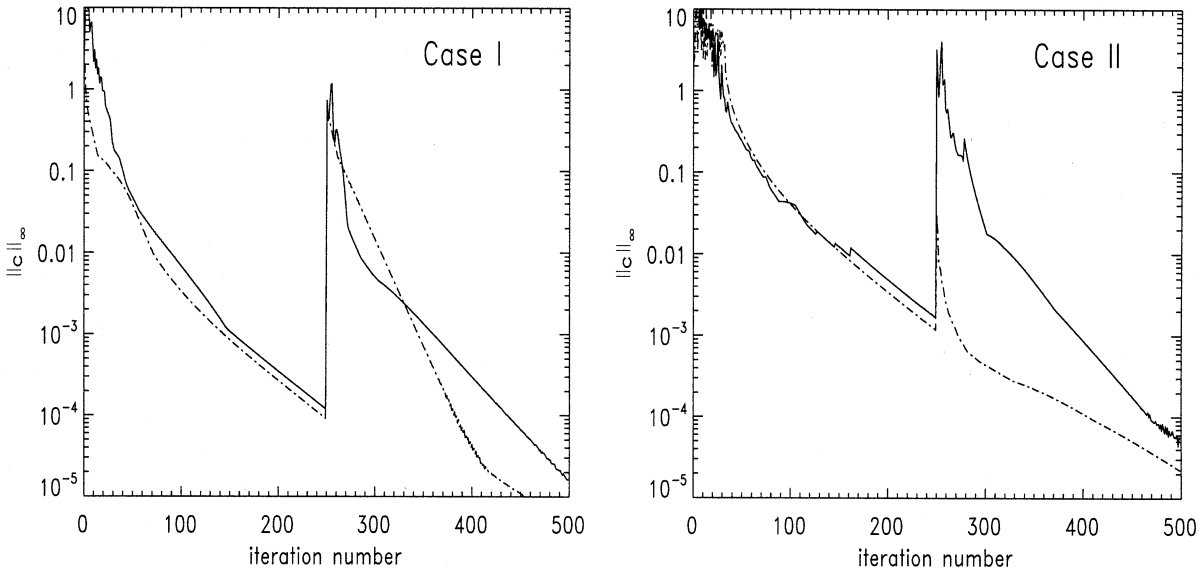

Fig. 1. Convergence rate for the (left) self-emitting test case and for the (right) illuminated slab case. The solid curves correspond to Stokes Q parameter while the dash-dotted ones to Stokes I. The almost vertical lines at iteration number 250 just indicate that a change of grid level is performed

core and logarithmically spaced in the line wing. The core-wing transition frequency x_c was set to 3.5 Doppler widths (see discussion in PA95, Sect. 5).

In both cases, we considered pure R_{II-A} redistribution in frequency which provides difficult test cases. For the computation of the redistribution matrix $\hat{g}$ we used the fast approximation of R_{II-A} given by Gouttebroze (1986).

Other input model parameters are the Voigt parameter $a = 10^{-3}$, the depolarization parameter $W_2 = 1$, the collisional destruction probability $\varepsilon = 10^{-6}$ and the Planck function B which is unity in CASE I and zero in CASE II.

5. Validation of the results

Results obtained with our new ALI-based code (PALIP) were compared to those given by a Feautrier code. Angular, spatial and frequency quadratures used in both codes are identical.

5.1. Convergence properties

To demonstrate the convergence behaviour of the PALIP method, we show in Fig. 1 the infinite norm of the relative correction from one iteration to the next. The latter correction is defined, as in Faurobert-Scholl et al. (1997) as

$$c_{I,Q}(x,\tau_k) = \frac{\mid \delta S_{I,Q}(x,\tau_k) \mid}{\frac{1}{2}(\mid S_{I,Q}(x,\tau_k) \mid + \mid S_{I,Q}(x,\tau_{k+1}) \mid)} \ . \qquad (23)$$

The infinite norm $\|c\|_\infty$ is the maximum value of the $c(x,\tau)$ matrix. Instead of displaying the convergence rate of each component of $\hat{S}$ we only consider those of the vector[2] $\boldsymbol{P}$ defined as

$$\begin{cases} P_I \equiv S_{11} + S_{12} \\ P_Q \equiv S_{21} + S_{22} \ . \end{cases} \qquad (24)$$

At each grid level we performed 250 iterations of the CRDCS scheme. $\hat{S}$ was initialized in each case with the respective primary source matrix $\hat{S}^*$. We also tried different initializations which all lead to the same solution although the first steps of the iterative process at grid level 1 are obviously different. Further, in order to demonstrate the favourable convergence property of PALIP, we did not implement acceleration of convergence (see Auer 1991).

It was already demonstrated in PA95 the good convergence property of the CRDCS scheme for the intensity component P_I. This can also be noticed in Fig. 1 where the behaviour of the maximum relative correction $\|c_I\|_\infty$ are displayed as the dash-dotted curves.

For the self-emitting slab test case, the decrease of $\|c_Q\|_\infty$ (the solid curve) is fairly smooth except maybe at the very start of the level-2 iterative process. However $\|c_Q\|_\infty$ decreases rapidly and reaches an asymptotic regime after 50 iterations. It can be noticed that $\|c_Q\|_\infty$ starts wiggling at large iteration numbers. This indicates that the source function increment have reached computer accuracy. The same shows on $\|c_Q\|_\infty$ for CASE II.

The evolution of $\|c_Q\|_\infty$ is more irregular during the first stage of the iterative process for the illuminated slab case both at

[2] Although our new code PALIP works with the matrix form of the source function, the Feautrier code we used for validating the results deals with the vector $\boldsymbol{P}$ and therefore does not give us access to each component of $\hat{S}$ but to the sum of each line of the source matrix.

grid level 1 and 2. These peaks in $\|c_Q\|_\infty$ come from very small values of the denominator of c_Q which can be of the order of computer accuracy at some depths. However, a smooth asymptotic regime is reached after 50 to 100 iterations are performed on any particular grid level.

5.2. About the solutions

The "fast converging" component P_I is in excellent agreement with results from the Feautrier code. The maximum relative error between the two sets of results does not exceed 5%.

As regards the polarized component of the source functions, comparisons between the Feautrier and PALIP solutions are displayed in Figs. 2 and 3 for cases I and II respectively; for symmetry reasons we only plot P_Q across one half of the slab. In both cases we selected two frequencies in each of the three frequency ranges: the Doppler core, the transition region (near wings) and the far wings. We indicate in Fig. 2 the reduced frequency x corresponding to each curve. The same frequency points are adopted for Fig. 3.

These graphs show clearly that, within graphic resolution, there is almost perfect agreement between the PALIP results (solid lines) and those from the Feautrier code (dashed lines).

We observe that the polarized component P_Q is negative in the surface boundary layer and goes through a positive maximum when the monochromatic optical depth $\tau\phi_x$ is of order unity. It decreases to zero at larger optical depths. In the case of a self-emitting slab, the driving term for the polarization is related to the anisotropy of the line radiation field by the frequency integration (see Faurobert 1988)

$$a(x,\tau) = \sqrt{\frac{1}{8}} \int_{-\infty}^{+\infty} \left[\frac{R_{xx'}}{\phi_x}\right] dx' \frac{1}{2} \int_{-1}^{+1} (1-3\mu^2) I_{x'\mu} d\mu \ . \quad (25)$$

The radiation field is limb-brightened for frequencies such that the monochromatic optical depth $\tau\phi_x/\mu$ is larger than unity, whereas it is limb-darkened for frequencies where this quantity is smaller than 1 (see Faurobert 1988). As a consequence the integral in Eq. (25) is the sum of two terms of opposite signs, namely, the positive contribution of optically thick frequencies and the negative contribution of optically thin frequencies. Close to the surface, the negative contribution dominates almost at all frequencies. When τ increases, the positive contribution of optically thick frequencies increases. It shows a maximum when the monochromatic optical depth is of order unity. At larger optical depths the anisotropy of the line radiation field decreases because of multiple scattering.

We notice that the order of magnitude of P_Q varies strongly from the core to the wings. The largest values are reached for frequencies at about 10 Doppler widths from line center. The corresponding monochromatic optical depth is unity for optical depths τ of the order of the thermalization length ($1/\varepsilon = 10^6$). At that depth the radiation field in the line core is isotropic; the negative contribution of the optically thick domain to Eq. (25) is thus very small.

In the case of an illuminated slab, the resonance polarization is driven by the anisotropy of the radiation field and by

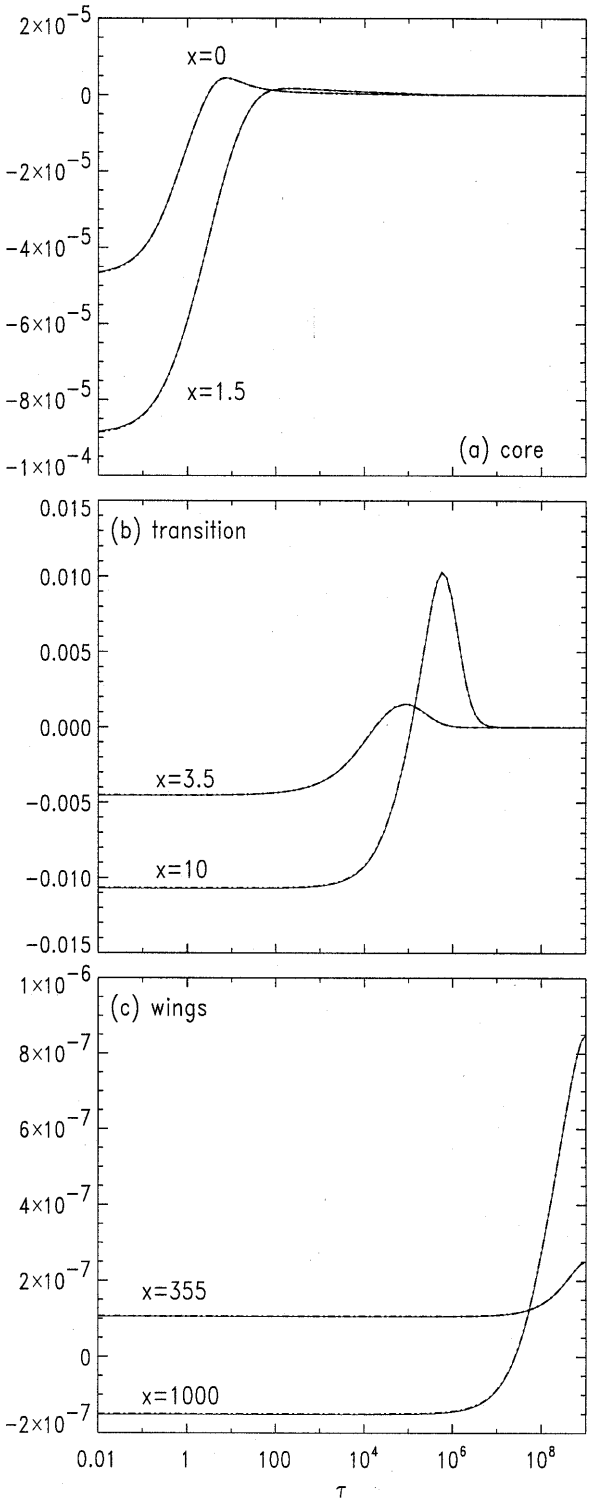

Fig. 2a–c. P_Q solutions obtained respectively with a Feautrier code and our new PALIP code are displayed in three different frequency domains: **a** core frequencies x = 0, 1.5 **b** transition to the wings x = 3.5, 10 and finally **c** wing frequencies x = 355, 1 000. PALIP results correspond to the solid curves and Feautrier ones to the thicker dashed lines; differences are almost undiscernible at graphics resolution

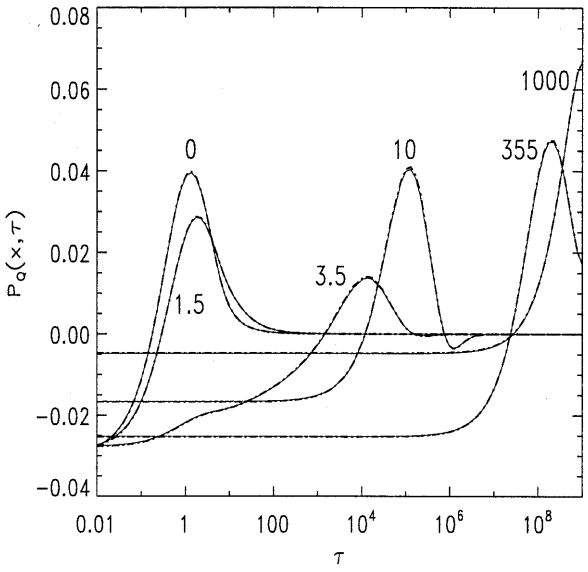

Fig. 3. Same as Fig. 2 but for the illuminated slab case. We display here the source functions at the same frequencies as the ones selected in Fig. 2. For increasing values of x the peak in P_Q moves towards slab center. The agreement between the two sets of results is excellent

the primary source term S^*_{22} defined in Eq. (21) due to the scattering of the incident radiation. For $\mu_0 = 0.5$, $p^{inc} = -0.20$ and $I^{inc} = 1$ this term is negative. For wing frequencies, where $\tau\phi_x/\mu_0 < 1$, we have $M(x,\tau,\mu_0) = 1$ and $S^*_{22} \simeq -0.07$. The behaviour of the anisotropy of the line radiation field is different from the self-emitting case. In the illuminated slab, the line intensity is strongly dominated by the incident radiation which propagates by multiple scattering down to optical depths of the order of the thermalization length. At depth τ, for optically thin frequencies the radiation field is essentially propagating inwards in the μ_0 direction; this yields a positive contribution to the integral in Eq. (25). For optically thick frequencies the preferred direction of propagation is lost because of the scattering of line photons. The line radiation field is limb-brigthened as in the self-emitting case; this yields a positive contribution too. The integral in Eq. (25) is thus positive. Since the incident radiation is independent of frequency, the order of magnitude of P_Q does not vary by a large factor for the different frequencies.

6. Conclusion

We have shown how the core-wing scheme for PRD proposed by Paletou & Auer (1995) for unpolarized non-LTE radiation transfer problems can be implemented in the Polarized Accelerated Lambda Iteration method of Faurobert-Scholl et al. (1997). We were able to treat two difficult test cases considering very thick isothermal slabs, pure R_{II-A} redistribution in frequency and no background absorption. Comparisons with results given by a Feautrier code are excellent. Moreover, the new PALIP code is much faster - at least a factor of 4 *without* acceleration of convergence - and requires much less computer memory.

We leave for a further study the two following issues: (a) implementation of optical depth grid adaptation and (b) detailed study of PALIP convergence and assessment of a rigorous stopping criterion (see e.g. Auer et al. 1994).

Besides, the CRDCS method can apply further to the case of polarization in a weak magnetic field regime. Indeed weak magnetic field regime can also be treated in the framework of PALI (Nagendra et al. 1997). Our preliminary tests of Hanle plus PRD effects computations are very promising.

Finally, we believe that the latter developments in the field of polarized radiation transfer are definitely of great interest in the perspective of interpreting new spectro-polarimetric data which will be collected with the THÉMIS telescope.

Acknowledgements. We wish to thank Drs H. Frisch and K.N. Nagendra for helpful discussions and comments.

References

Auer L.H., 1991, in *Stellar Atmospheres: Beyond Classical Models*, Eds. Crivellari, Hubený & Hummer, NATO ASI Series, Kluwer
Auer L.H., Fabiani Bendicho P., Trujillo Bueno J., 1994, A&A 292, 599
Auer L.H., Paletou F., 1994, A&A 285, 675
Dorfi E.A., Drury L.O., 1987, J. Comput. Phys. 69, 175
Faurobert M., 1987, A&A 178, 269
Faurobert M., 1988, A&A 194, 268
Faurobert-Scholl M., 1992, A&A 258, 521
Faurobert-Scholl M., 1994, A&A 285, 655
Faurobert-Scholl M., Frisch H., Nagendra K.N., 1997, A&A 322, 896
Gouttebroze P., 1986, A&A 160, 195
Hummer D.G., 1962, MNRAS 125, 21
Ivanov V.V., 1995, A&A 303, 609
Ivanov V.V., Kasaurov A.M., Loskutov V.M., Viik T., 1995, A&A 303, 621
Jefferies J.T., 1968, *Spectral Line Formation*, Blaisdell, Waltham, Mass.
Mihalas D., 1978, *Stellar Atmospheres*, Freeman, San Francisco
Nagendra K.N., Frisch H., Faurobert-Scholl M., 1997, *"An operator perturbation method for polarized line transfer III. Hanle effect in 1D media"*, preprint
Olson G.L., Auer L.H., Buchler J.R., 1986, J. Quant. Spectrosc. Radiat. Transfer 35, 431
Paletou F., 1995, A&A 302, 587
Paletou F., Auer L.H., 1995, A&A 297, 771
Rees D.E., 1978, PASJ 30, 455
Rybicki G.B., Hummer D.G., 1991, A&A 245, 171
Scharmer G.B., 1983, A&A 117, 83
Väth H.M., 1994, A&A 284, 319

This article was processed by the author using Springer-Verlag LaTeX A&A style file *L-AA* version 3.